Met. Mater. Int., Vol. 16, No. 3 (2010), pp. 483~488
doi: 10.1007/s12540-010-0621-7 Published 26 June 2010

Cracking Behavior in a Dissimilar Weld between High Silicon Nodular Cast Iron and Ferritic Stainless Steel

Sanghoon Kim[1], Sangchul Lee[1], Kyutae Han[1], Seunggab Hong[2], and Changhee Lee[1,*]

[1] Div. of Mater. Sci. and Eng., Hanyang Univ.,
17 Haengdang-dong, Seongdong-gu, Seoul 133-791, Korea
[2] POSCO Technical Research Lab,
1, Geodong-dong, Nam-gu, Pohang-si, Gyeongbuk 790-785, Korea

(received date: 2 January 2009 / accepted date: 28 December 2009)

In this work, the microstructural evolution and cracking behavior of a dissimilar weld between high silicon nodular cast iron and ferritic stainless steel was investigated. An austenitic filler metal (Y309) was employed to produce the dissimilar weld. Microstructural analysis revealed that cracking formed at the unmixed zone (UMZ) and propagated into the partially melted zone (PMZ) in the bond line between the cast iron and the Y309, with hard layers formed around the bond line. The cracking behavior was strongly related to the difference in the melting points of cast iron and the Y309 filler metal, the local liquation of the laves phase, and the constitutional liquation between the graphite and austenite phases in the PMZ.

Keywords: alloys, welding, phase transformation, scanning electron microscopy (SEM), hot cracking

1. INTRODUCTION

Materials that are used in automobile exhaust systems have to be selected very carefully due to the high operating temperature and strong acidic atmosphere. In addition, an exhaust manifold has a complicated shape and a reduction in its weight is necessary for energy savings and environmental conservation. Considering these factors, heat-resistant nodular graphite cast irons and ferritic stainless steels are currently used in exhaust manifolds. As such, studies regarding the microstructures and mechanical properties of these materials have been conducted by many researchers [1-6]. Also, it is accepted that nodular cast iron and stainless steel form an optimum combination for the construction of exhaust manifold components.

Dissimilar welding between cast iron and ferritic stainless steel is one of the important process technologies for assembling the exhaust system. Several researchers have reported on the formation of an unmixed zone (UMZ) in the bond lines of dissimilar welds. The UMZ, which has unique properties, can be formed during welding by the solidification of a completely melted base metal, which is not mixed with the weld metal. The chemical composition of the UMZ is identical to that of the base metal and is very narrowly formed along the fusion line. In addition, the chemical/mechanical properties of the UMZ have been found to deteriorate when compared to those of the base metal. This is due to the dendritic structure of the UMZ formed by rapid melting and cooling processes [7-10]. Such a structure generally includes segregation. Furthermore, hot cracking frequently occurs in the partially melted zone (PMZ) and the heat affected zone (HAZ) due to metallurgical reactions between the secondary phase and the matrix [11-13]. However, few studies have been done regarding the microstructural properties and cracking behavior in dissimilar welds between cast iron and stainless steel.

In this work, the microstructural properties in a dissimilar weld between high silicon nodular cast iron (HiSiMo) and ferritic stainless steel (409L) are investigated.

2. EXPERIMENTAL PROCEDURE

In this study, high silicon nodular cast iron (HiSiMo) and a ferritic stainless steel (409L) were used to create a dissimilar weld with an austenitic filler metal (Y309). The chemical compositions of the base and filler metals are given in Table 1. Welding was performed using a GMAW process with 1.7 kJ/cm of heat input and Ar-2%O_2 shielding gas. Optical microscopy (OM) and scanning electron microscopy (SEM) were carried out to analyze the microstructures and cracks in the weld. To observe the microstructure, 2 % nital for

*Corresponding author: chlee@hanyang.ac.kr

Table 1. Chemical compositions of the base metals and filler metal

Base metals	C	Si	Mn	Mo	Mg
HiSiMo	3.12	4.0	0.16	0.9	0.03
	C	Cr	Si	Mn	Ti
STS409L	0.01	11.26	0.56	0.29	0.19
Filler metal	C	Ni	Cr	Mn	Si
Y309	0.03	13.00	24.2	1.57	0.46

HiSiMo and a mixture of acids (HCl, HNO_3, and acetic acid) for the stainless steels were used. Phases were identified through transmission electron microscopy (TEM), electron probe micro-analysis (EPMA), and energy dispersive spectroscopy (EDS). To prepare the TEM specimens, a thin disc of HiSiMo was electro-polished using a mixture of 5 % perchloric acid and 95 % methanol. Differential thermal analysis (DTA) and thermal cycling tests using a Gleeble system were performed in order to confirm the melting sequence and the melting temperature of HiSiMo. The solidus and liquidus temperatures at several positions in dissimilar welds with different compositions were calculated using the Thermo-Calc. program. Hardness values, attained using a Vickers hardness tester, were measured in macro and micro regions in order to analyze the local mechanical properties.

3. EXPERIMENTAL RESULTS

3.1. Microstructural analysis of the base metal (HiSiMo)

HiSiMo possesses a high content of both silicon and molybdenum, which serve to improve the high temperature oxidation resistance and the fatigue properties. The addition of Si promotes carbon graphitization due to the increased chemical potential of carbon. A minute Mg content in HiSiMo is effective for the spherodization of graphite. The microstructure of HiSiMo consists mainly of ferrite and nodular graphite, and thus it has a good balance of strength and toughness. As shown in Fig. 1(a), the microstructure of the HiSiMo used in this study consists of a ferrite matrix, nodular graphite, and a small amount of pearlite. Various phases are also observed at the solidification grain boundaries, as shown in Fig. 1(b). Through the results of OM, the existences of pearlite, martensite, and eutectic phases are confirmed at the solidification grain boundary. Figure 2 shows the results of EPMA analysis at the solidification grain

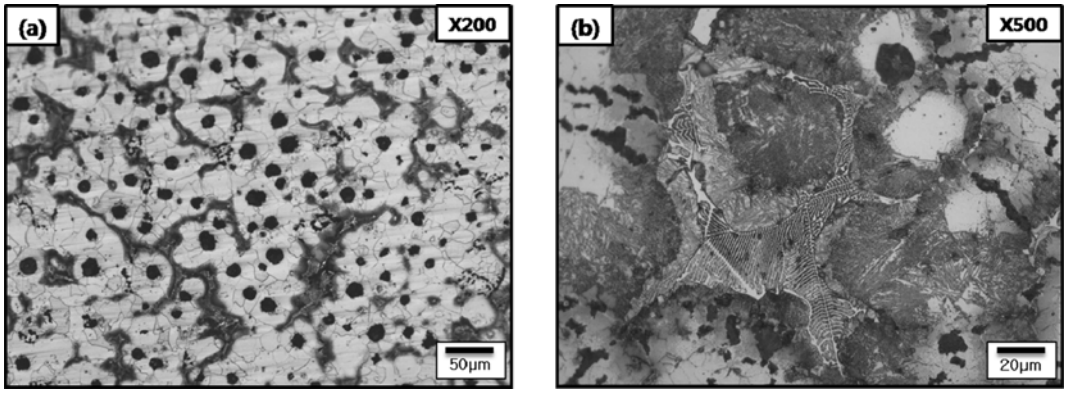

Fig. 1. OM images of the base metals: (a) HiSiMo and (b) Solidification grain boundary of HiSiMo.

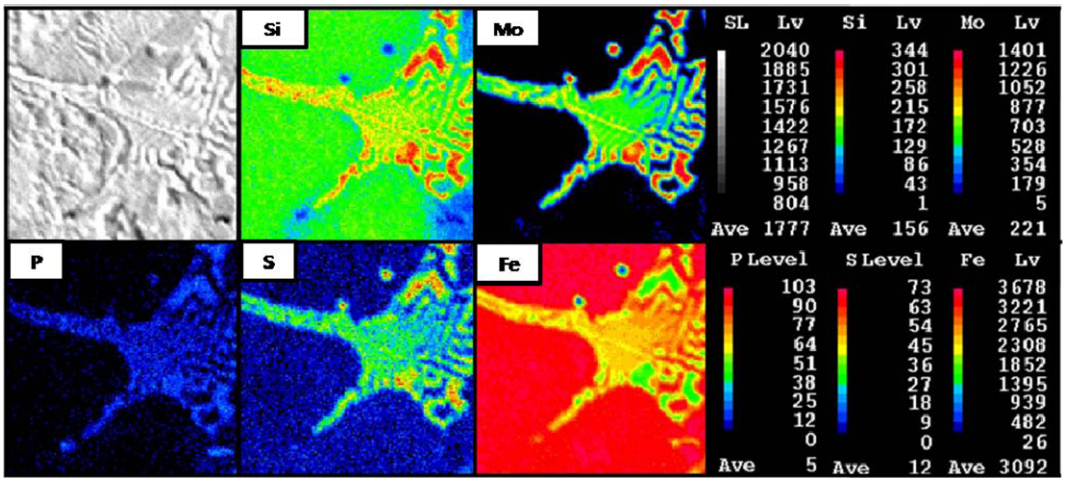

Fig. 2. EPMA data for the eutectic phase at the solidification grain boundary.

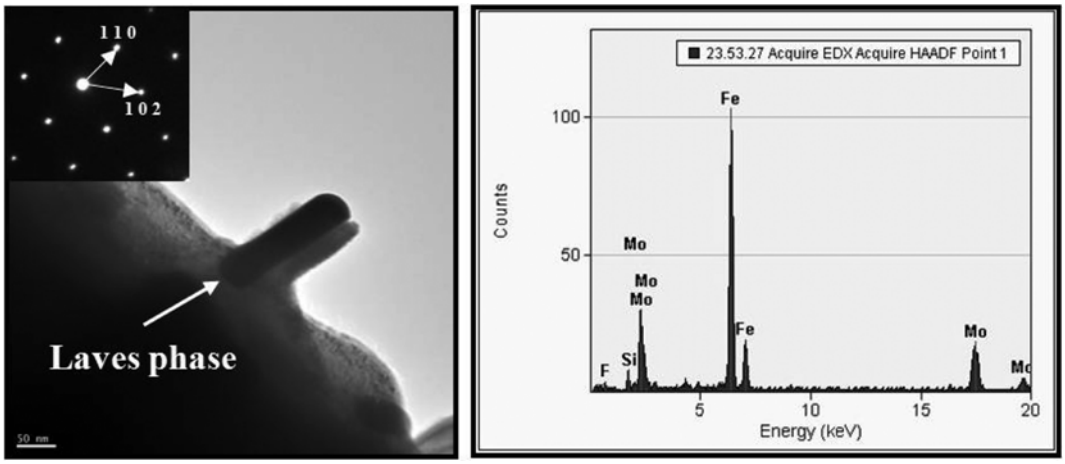

Fig. 3. TEM image and EDS data for the $Fe_2(Mo,Si)$ laves phase.

boundary. The eutectic phase, in particular, has very high contents of Mo and Si. Such a result may indicate the presence of an $Fe_2(Mo,Si)$-type laves phase. Figure 3 shows the results of TEM and EDS analyses of the eutectic phase in the HiSiMo base metal, showing that the eutectic phase is an $Fe_2(Mo,Si)$ laves phase with an HCP crystal structure. These $Fe_2(Mo,Si)$ laves phases are distributed mainly at the solidification grain boundary. Furthermore, relatively high concentrations of S and P are also detected in the eutectic phase due to segregation during casting.

3.2. Thermal analysis of the base metal (HiSiMo)

The DTA curve in Fig. 4 shows several peaks that are related to various phase transformation temperatures. The first peak appears near 800 °C and is the ferrite to austenite phase transformation temperature. The last two peaks, observed near 1160 °C and 1210 °C, represent the solidus and liquidus temperatures, respectively. Two additional peaks near 1110 °C and 1140 °C could not be verified through the DTA curve. Thus, to assure phase transformations near 1110 °C and 1140 °C, thermal testing was carried out using a Gleeble system. Every thermal test specimen was heated to each peak temperature at the same heating rate used in the DTA analysis. The specimens were then quenched in water. Figure 5 shows the OM results of the thermal test specimens that were water quenched at 1100 °C, 1120 °C, and 1150 °C. No melting reactions are observed for any phases in the 1100 °C water-quenched specimen. However, in the 1120 °C water-quenched specimen, melting of the eutectic phase at the solidification boundary was observed. In the 1150 °C water-quenched specimen, the melting region extended to graphite. Through these results, it can be stated that the phase transformation near 1110 °C represents the eutectic reaction temperature between the $Fe_2(Mo,Si)$ laves phase and the austenite, and 1140 °C is the eutectic melting temperature of the graphite and austenite matrix.

3.3. Microstructure of the fusion line

As shown in Fig. 6, a crack exists at the bond line between the HiSiMo and the Y309. Various microstructures were

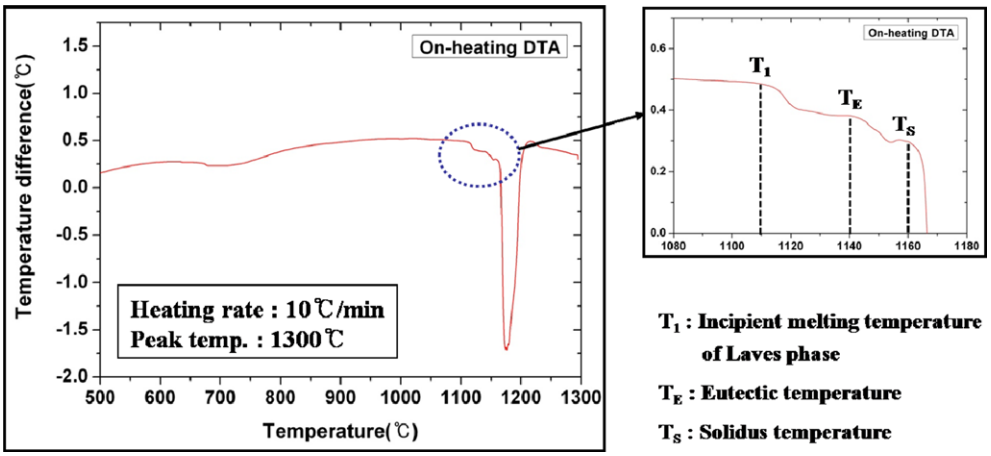

Fig. 4. DTA curves for the HiSiMo base metal.

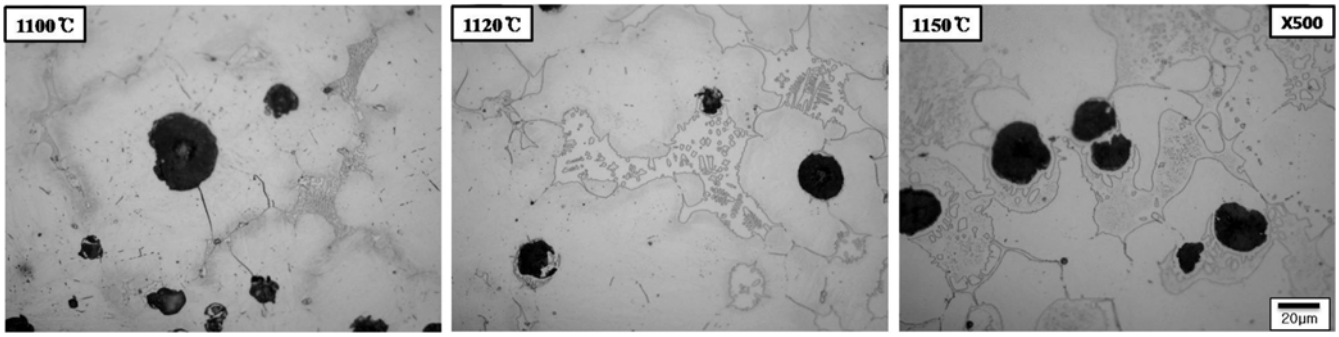

Fig. 5. OM images of thermal test specimens that were water quenched at 1100 °C, 1120 °C, 1150 °C.

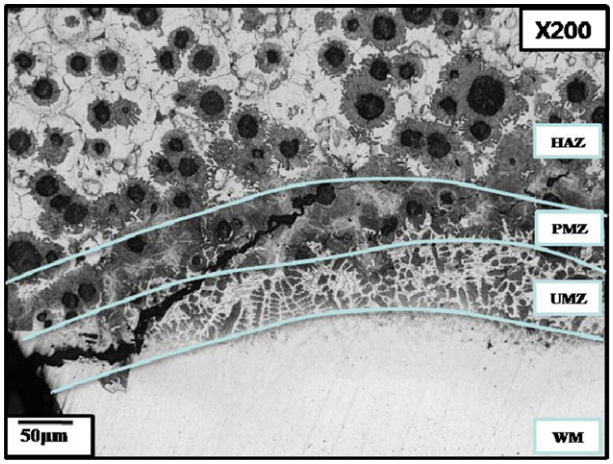

Fig. 6. A crack formed at the bond line.

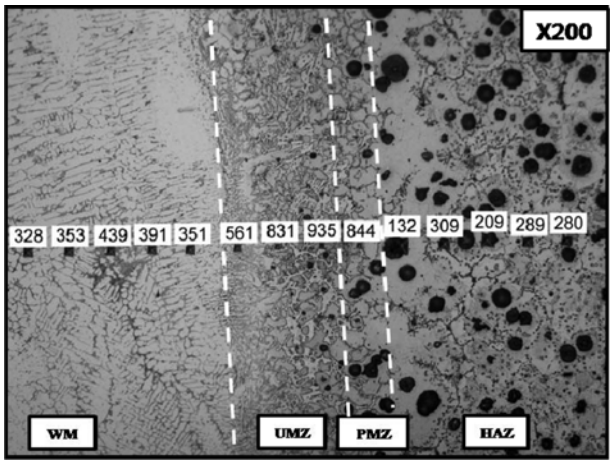

Fig. 7. OM image and hardness test results for the bond line.

formed at the bond line based on the peak temperature (distance from the fusion line). The dissimilar weld exhibits a UMZ microstructure that is similar to that found in many previous dissimilar welds [7-10], with the crack initiating at the UMZ and growing into the PMZ.

Figure 7 shows the microstructures and hardness profile across the bond line. The UMZ and PMZ have the highest hardness. In the case of the HiSiMo-Y309 bond line, a hard layer consisting of carbide and martensite phases formed as a result of the dissolution of nodular graphite and diffusion of carbon in the UMZ, PMZ, and HAZ. As such, the hardness increased with an increase in the peak temperature due to the increased carbon content in the microstructure. The chemical composition of the UMZ is identical to that of the base metal, except that UMZ has a very high content of carbon due to the full dissolution of graphite in the rapidly solidified dendritic structure. Thus, the final microstructures consist of martensite and cementite. In addition, the degree and width of the carbon-diffused layer formed around the nodular graphites in the PMZ and HAZ vary as a function of the distance (peak temperature) from the fusion line.

To understand the mechanism of crack formation at the HiSiMo-Y309 bond line, a fractured surface was observed

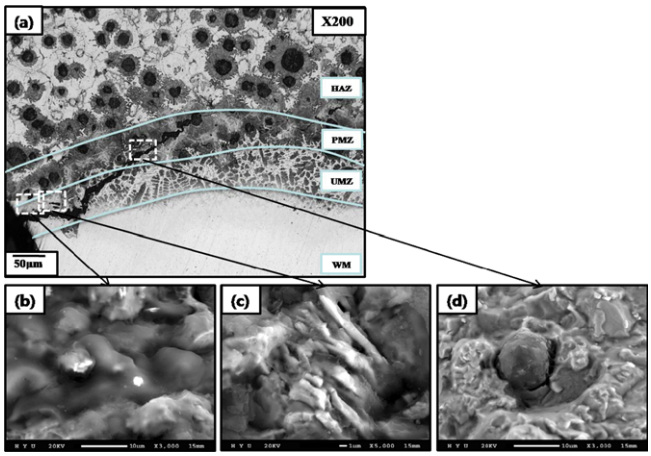

Fig. 8. (a) OM image of a crack at the bond line. Evidence of melting and re-solidification near the origin of crack can be observed. (b) Smooth dendritic structure at the UMZ. (c) Eutectic phase at the UMZ. (d) Melting traces near graphite at the PMZ.

by SEM. Figures 8(b), (c), and (d) shows a representative microstructure observed for the fractured surface. Evidence of the existence of liquid at the moment of crack formation can be expected from the smooth dendritic structure (Fig. 8(b)) and the eutectic phase (Fig. 8(c)).

Thus, it is assured that hot cracking occurred during the welding process.

4. DISCUSSION

4.1. Crack initiation at the UMZ

As observed above, a crack was initiated at the UMZ and propagated through the grain boundaries in the PMZ (Fig. 6). Crack formation at the UMZ may be attributed to the difference in the solidification temperatures between the UMZ and the Y309 weld metal. The calculated melting temperatures at several positions (chemical compositions of 25 %, 50 % and 75 % mixed regions with filler metal were assumed), including the UMZ in the dissimilar weld fusion line, are shown in Fig. 9. The difference in the solidus and liquidus temperature between the UMZ and the Y309 weld metal is found to be approximately 250 ℃. Therefore, during solidification, the UMZ remained in a liquid phase even after the complete solidification of the Y309 filler metal and the partially mixed region. As a result, a crack could form at the UMZ of the HiSiMo due to shrinkage stress in the weld metal.

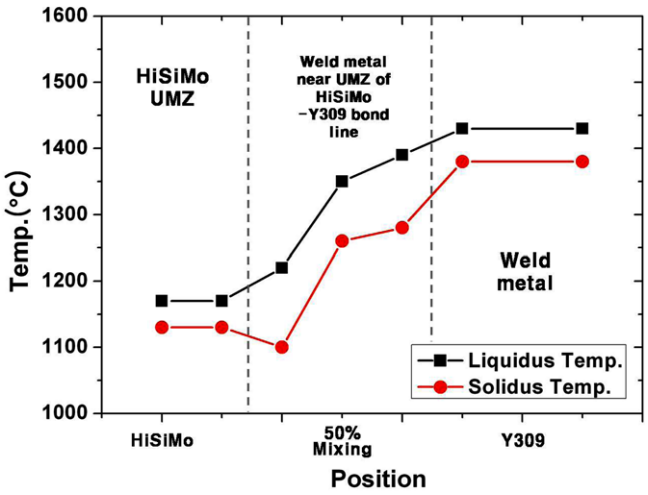

Fig. 9. Calculated solidus and liquidus temperatures.

4.2. Crack propagation at the PMZ

After crack initiation at the UMZ, the crack mainly propagated through the melted grain boundaries in the PMZ. As shown previously in Fig. 4, the eutectic temperature between the laves phase and the austenite is lower than the melting temperature of the matrix. Consequently, the liquid phase, which was formed by a eutectic reaction between the laves phase and the austenite matrix, penetrates into the grain boundaries because the $Fe_2(Mo,Si)$ laves phase exists at the solidification grain boundary. Thus, after welding, the eutectic constituent formed by the eutectic reaction between the laves phase and the austenite in the PMZ can be observed through SEM imaging. As shown in Fig. 10, high concentrations of Mo and Si in the eutectic constituent were also detected using EPMA.

A crack initiated at the UMZ can also propagate through the liquid phase that was formed by the constitutional liquation between the graphite and austenite phases around the graphite. Constitutional liquation is one of the main factors that causes liquation cracking; it occurs due to rapid heating during welding [11,12]. According to the literature, constitutional liquation in HiSiMo is caused by liquation near the graphite. That is, constitutional liquation is localized melting near the graphite and occurs due to a eutectic reaction between graphite and austenite [14,15]. Strong evidence of this phenomenon is shown in Fig. 8(d). During rapid heating, carbon diffuses from the graphite into the austenite. As such, the content of carbon in the austenite near the graphite can reach the solubility limit of austenite. A eutectic reaction between the carbon-rich austenite and the graphite can then take place. Liquation can then occur at a temperature that is lower than the solidus temperature. This constitutional liquation is also observed in the simulated weld specimen that is subject to the same severe heating rate of real welds using a Gleeble system. The melting trace like a ring near the graph-

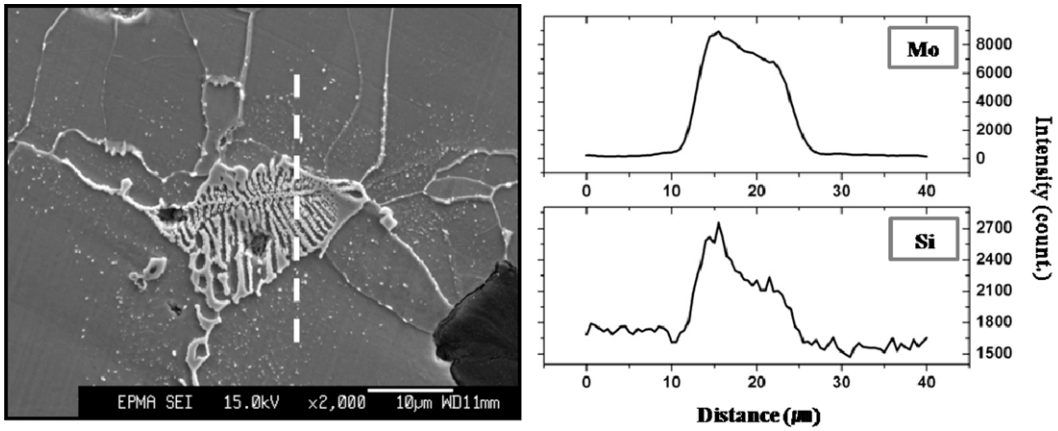

Fig. 10. SEM images of the eutectic constituent and the EPMA line scanning results.

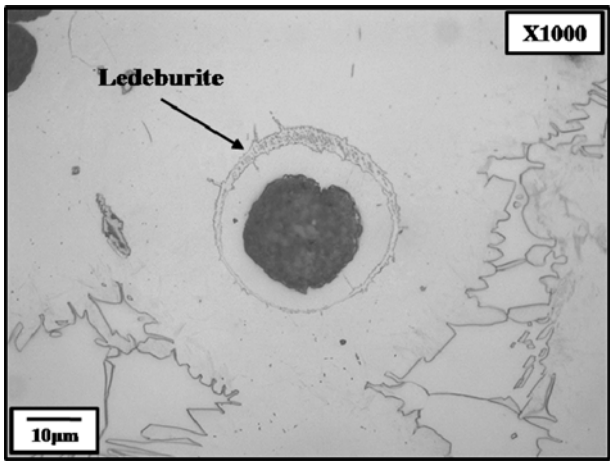

Fig. 11. OM image of the melting trace by constitutional liquation near graphite.

ite is shown in Fig. 11. This melting trace consists of martensite and carbide phases and is formed by the rapid cooling of austenite and carbide from a high temperature during welding. This rapidly cooled eutectic phase is called 'Ledeburite' and provides good evidence of localized melting by constitutional liquation.

Through the above results, it was verified that a crack mainly propagates along the solidification grain boundary at the PMZ and propagates through the liquid phase around the graphite. However, due to the constitutional liquation of graphite, the crack propagation area is observed in relatively narrow regions when compared to the area arising from the liquation behavior of the Fe_2(Mo,Si) laves phase. Such findings are due to the difference in the solidification temperature ranges of the liquid phases that are formed by the liquation behavior of the Fe_2(Mo,Si) laves phase and the nodular graphite. The solidification temperature range of the liquid phase that is formed by the liquation of the Fe_2(Mo,Si) laves phase (>1110 °C) is wider than that of the liquid phase that is formed by the constitutional liquation of graphite (> 1140 °C).

5. CONCLUSIONS

In this study, a dissimilar weld for an exhaust manifold was formed by welding high silicon nodular cast iron (HiSiMo) and ferritic stainless steel (409L) using an austenitic stainless steel filler metal (Y309). The microstructure and cracking behavior of the dissimilar weld was then analyzed.

After welding, a crack was observed at the bond line between the HiSiMo and Y309. The crack originated at the UMZ and propagated along the PMZ. Depending on the peak temperature, various microstructures, such as the UMZ, PMZ, and HAZ, were formed at both bond lines. In addition, at the HiSiMo-Y309 fusion line, a hard layer was formed by the dissolution and diffusion of nodular graphite and the subsequent rapid cooling during welding.

Cracks in the UMZ and PMZ of the HiSiMo-Y309 bond line were confirmed due to hot cracking and were initiated by the difference in melting temperature between the HiSiMo and the filler metal. The crack was propagated by a eutectic reaction between the laves phase and the austenite matrix and by the constitutional liquation between the graphite and the austenite phase.

ACKNOWLEDGMENTS

The authors would like to acknowledge the financial support of POSCO Technical Research Laboratory.

REFERENCES

1. M. Takanezawa, Y. Tomota, and Y. Kobayashi, *ISIJ Int.* **38**, 106 (1998).
2. H. Ishikawa, *CAMP-ISIJ* **4**, 1760 (1991).
3. T. K. Ha, H. T. Jeong, and H. J. Sung, *J. Mater. Process. Tech.* **187-188**, 555 (2007).
4. S. H. Park, Y. D. Lee, and Y. Y. Lee, *J. Kor. Inst. Met. & Mater.* **33**, 1323 (1995).
5. D. Kim and H. Kim, *J. Kor. Inst. Met. & Mater.* **46**, 652 (2008)
6. J. P. Kong, T. J. Park, H. S. Na, J. K. Kim, S. H. Uhm, I. S. Woo, J. S. Lee, and C. Y. Kang, *Kor. J. Met. Mater.* **48**, 297 (2010).
7. Sindo Kou, *Welding Metallurgy*, *2nd ed*., John Wiley & Sons, New Jersey (2003).
8. W. A. Baeslack, III, J. C. Lippold, and W. F. Savage, *Weld. J.* **58**, 168s (1979).
9. C. D. Lundin, W. Liu, G. Zhou, and C. Y. P. Qiao, *Unmixed Zone in Arc Welds: Significance on Corrosion Resistance of High Molybdenum Stainless Steels*, Welding Research Council, New York (1998).
10. M. D. Rowe, T. W. Nelson, and J. C. Lippold, *Weld. J.* **78**, 31s (1999).
11. J. J. Pepe and W. F. Savage, *Weld. J.* **46**, 411s (1967).
12. B. H. Yoon, Y. S. Ahn, and C. H. Lee, *ISIJ Int.* **42**, 178 (2002).
13. I. S. Woo and K. Nishimoto, *Met. Mater. Int.* **7**, 241 (2001).
14. J. Grum and R. Šturm, *Mater. Charact.* **37**, 81 (1996).
15. J. Grum and R. Šturm, *Appl. Surf. Sci.* **187**, 116 (2002).